BJRS

BRAZILIAN JOURNAL
OF
RADIATION SCIENCES
09-02C (2021) 01-16

# Digital processing of images with defects due to double beam attenuation in indirect X-ray fluorescence mapping

Silva[a] L. D., Souza[b] L. C., Oliveira[c], D. F., Anjos[b], M. J., Gonçalves[a], E. A. S*

[a]*Instituto Federal do Rio de Janeiro, 26600-000, Rua sebastião Lacerda S/N sala S28, Centro, Paracambi.*

[b]*Universidade do Estado do Rio de Janeiro, 20943-000, São Francisco Xavier, 524, Maracanã, Rio de Janeiro*

[c]*Universidade Federal do Rio de janeiro, 21941-914, Av Horácio Macedo,2030 - Ilha do fundão, Rio de Janeiro*

* *elicardo.goncalves@ifrj.edu.br*

## ABSTRACT

**This work is based on the adaptation of a commercial X-ray fluorescence mapping equipment to map the transmission of characteristic X-ray beams through a sample. This adaptation was made without physical adjustments to the equipment, working only on the measurement and data processing parameters. The arrangement of the equipment's components causes not only the primary beam to pass through the sample, but also the resulting characteristic X-rays, causing a double attenuation and a defect in the final image known as ghosting. In this approach, a rudimentary genetic algorithm was developed using artificial images with simulated defects. This algorithm showed the characteristics of the convolution matrix K needed to solve the problem. The results show the real possibility of using the equipment for this adapted measurement and a methodology that can be expanded to different situations.**

***Keywords: Digital image processing, genetic algorithm, X-ray transmission.***

ISSN: 2319-0612
Accepted: 2021-07-13

## 1. INTRODUCTION

The X-ray fluorescence, or simply XRF, is a non-destructive analytical technique capable of performing a quick and relatively simple elemental analysis. It is based on the ionization of atoms in a sample, usually using a primary X-ray beam, and the measurement of the consequent characteristic X-rays generated from the ionized atoms [1]. This technique is well known and widespread in several fields of study.

X-ray fluorescence mapping equipment uses automation mechanisms to scan a given area of the sample, measuring it at small, regularly spaced points (spotsizes). The result is the elementary mapping of the measured region, usually presented in the form of one or more images [2].

Modern mapping equipment can split the sample into spotsizes of a few micrometers in diameter (micro XRF mapping) and make the measurement in a reasonably short time, using sophisticated automation techniques, extremely efficient components, and optimization of the acquisition process. There are many commercially available equipments for this type of measurement [3].

In most applications, the sample is placed on a platform where the X-ray beam is focused to ionize its atoms. The mapping can occur by moving the x-ray tube or, more commonly, by moving the platform with the sample. In some cases, it may be necessary to position a base or some fixture for the best positioning and fixation of the sample. If the sample is very thin, it is possible that the x-ray beam also ionizes atoms in this base. This would cause detection of characteristic x-rays not only from the sample but also from the base, creating unwanted noise.

But by adapting this way of measuring, this noise can be used for another characterization of the sample: by the arrangement of the components of this equipment (figure 1A), the characteristic x-ray beams generated in the base need to pass through the sample to reach the detector and are attenuated by it. This attenuation provides information about the sample.

By choosing bases with certain materials (e.g. metals), the energy spectrum of the characteristic X-rays would be composed of one or more peaks with well-defined energies [4], and can be treated, with good approximation, to photon beams with discrete energies. By detecting this signal, characterizing its intensity and energy, a transmittance measurement is made along this sample, which can be used to calculate different properties [5,6]. In this sense, the equipment, despite not being built for this purpose, can be used for mapping these properties.

In principle, this adaptation, which would not need to change any physical structure of the equipment, can take advantage of the automation, precision, and sophistication of the equipment to create a way to measure the attenuation of the sample, without any kind of cost or mischaracterization of the equipment.

The big difficulty is the direction of the primary x-ray beam: in this type of equipment, the tube is positioned in such a way that the primary beam must pass through the sample to create characteristic x-rays at the base. These characteristic x-rays will again pass through the sample towards the detector (figure 1B). This double crossing makes therefore a double attenuation, which due to the angulation of the components, takes place at slightly different points. Thus, each measured point carries the sample information twice, from slightly offset points.

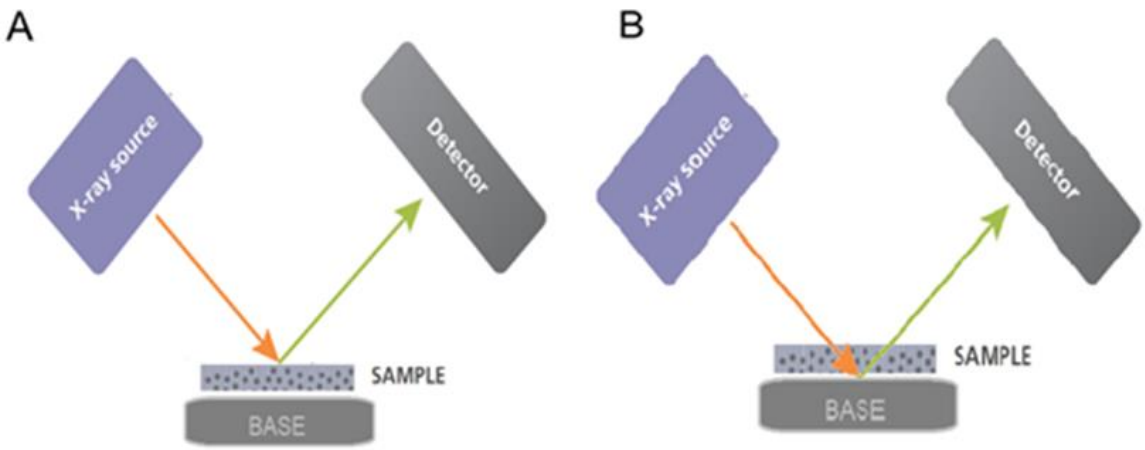


**Figure 1:** Difference between X-ray fluorescence measurement: (A) on the sample and (B) on the base (B).

This causes a double attenuation problem that results in two overlapping images in the output.

These results have the characteristics of images with a defect known as ghosting, which can be understood as the overlapping of two identical images, but displaced by a few pixels, as shown in figure (2).

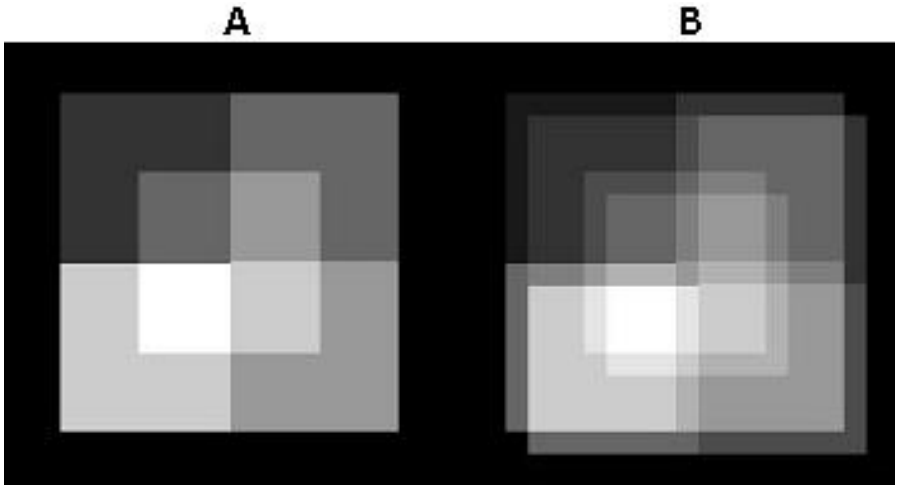


**Figure 2:** Example image without (A) and with (B) ghosting.

The goal of this work is to find a mathematical procedure that digitally removes this defect to find the optimal image. To do that, images were artificially generated and added ghosting to train a computational procedure so as to evaluate on how well it performs in removing the defect. The process is a rudimentary genetic algorithm [7], built specifically for this problem, and which reached satisfactory conclusions.

## 2. MATERIALS AND METHODS

In this work, the image I with ghosting is considered as the result of the two-dimensional convolution of an original image $I_0$ by a convolution matrix K.

$$I=I_0*K \tag{1}$$

Thus, to do the reverse process, the deconvolution, and from I, find $I_0$, it is necessary to know K. The two-dimensional deconvolution method used was Wiener's method [8,9]. For two-dimensional data, this was the only deconvolution method available in GNU Octave.

A small computational routine was used to create numerous random images, with artificially added ghosting, simulating that identified in the original data, to train an elementary genetic algorithm to find the K matrix.

### 2.1. Artificial Ghosting

Artificial images were created from randomly choosing pixels to be filled with colors that were also random. To vary some geometric features without much computational cost, the painted pixels occupied rectangular shapes (Figure 3A).

To create a displaced image $I_d$ from the original image $I_0$, it was sufficient to make each pixel of this new $I_d(R,C)$ in row R and column C equal to one pixel of the old image plus one displacement.

$$I_d(R,C) = I_0(R+\Delta R, C+\Delta C) \quad (2)$$

Where the values of ΔR and ΔC are the horizontal and lateral image displacements.

The image with the ghost I is the junction of the original image $I_0$ with the shifted image $I_d$ (figure 3B). This junction can obey any mathematical function between the values of each pixel of $I_0$ and $I_d$. A function that simulates as realistically as possible the behavior of the attenuation of the radiation beam was constructed.

$$I(L,C) = f(I_0(R,C), I_d(R,C)) \quad (3)$$

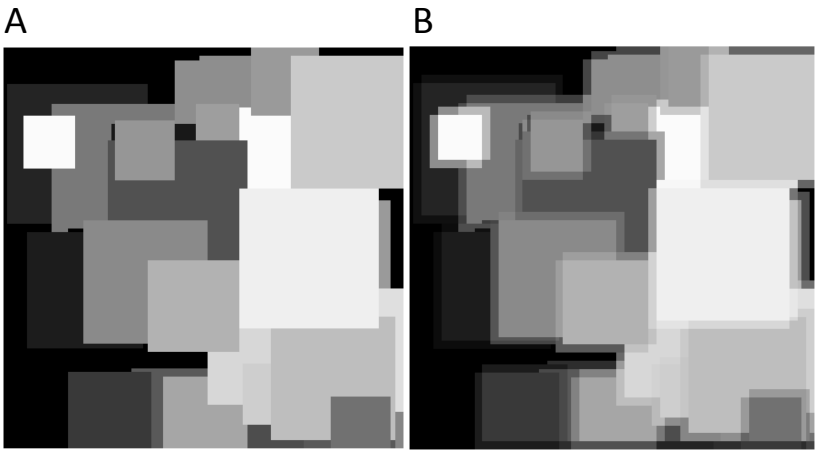


**Figure 3:** Example of an artificially created image.

The attenuation of a radiation beam obeys the Beer-Lambert's law [10]:

$$A = A_0 \exp(-\mu x) \quad (4)$$

Where A and $A_0$ are the final and initial beam intensities, respectively, μ is the attenuation coefficient and x is the thickness of the material passed through. The Octave image processing functions consider that when a pixel has a minimum value, this pixel is completely black; when it has a maximum value, it is completely white. This means that we must use an inverted scale between the pixel intensity I and the beam intensity A, i.e., I equals the maximum value of A, which by the equation is $A_0$, minus the beam intensity A for the given pixel.

$$I = A_0 - A \tag{5}$$

Therefore, the higher the beam intensity at a given point, the lower the pixel value and the closer to black (zero) the color of that pixel will be. Substituting equation (4) into equation (5):

$$I = A_0[1 - \exp(-\mu x)] \tag{6}$$

Thus, each pixel has a value directly proportional to I. The reasoning can be generalized for the two attenuations: of the primary beam towards the base and of the characteristic x-ray beam towards the detector. Each has an effective attenuation coefficient.

$$I = A_0[1 - \exp(-\mu_1 x_1)\exp(-\mu_2 x_2)] \tag{7}$$

Where $x_1$ and $x_2$ are the thicknesses of the sample points with effective coefficients $\mu_1$ and $\mu_2$, traversed by the primary and characteristic X-ray beams, respectively.

To normalize, and consequently optimize the image contrast, we need the pixel values to be between 0 and 1 (totally black and totally white). For this purpose, $A_0$ is assumed to be equal to 1. For the case of expression (3), considering that the primary beam and the characteristic X-rays are proportional and have different attenuation coefficients, but that their effective value does not suffer considerable variation along the sample:

$$I(L,C) = 1 - \exp[-\mu_1 I_0(R,C) - \mu_2 I_d(R,C)] \tag{8}$$

Equation (8) shows how the pixel values of image $I_0$ and $I_d$ are used to calculate the values of the artificial image with ghosting I, at the pixel in row R and column C.

### 2.2. Computational Simulation

#### 2.2.1 Genetic Algorithm

In the problem addressed, the desired matrix K, initially thought to have the same size as I and $I_0$, was treated as a genetic code. The value of each element of this matrix is a genetic unit (gene). Each candidate in Matrix K is treated, by the algorithm, as an individual. The algorithm, which is a rudimentary form of genetic algorithm, created mutations in these individuals, used the genes of the parent individuals to create the offspring, and performed artificial selection, favoring the fittest to convolve in the desired way.

The artificial images $I_0$, as well as their ghosted I, are used in the classification process for efficiency. In this work, each generation was composed of 100 individuals, arranged in a 10x10 table (figure 4A). Each of these individuals is tested for its ability to find image I from image $I_0$ by the convolution process. The 10 best individuals are selected to build the new generation (Figure 4B) by mixing their genes, pairwise, (Figure 4C), in a rudimentary process of crossing over. The new generation also undergoes small genetic mutations compared to the previous one.

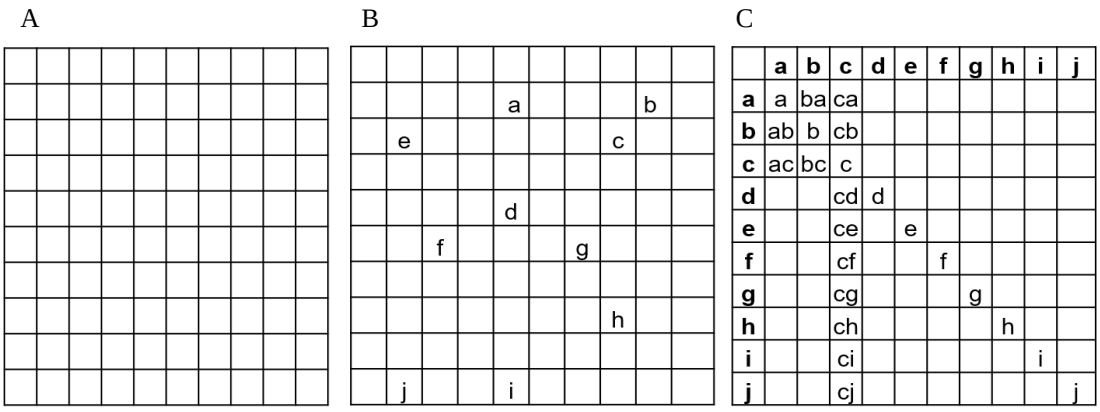


**Figure 4:** From a population of 10x10 invidivuals (A) the ten best are selected (B) to recombine and create the next generation (C).

#### 2.2.2 Artificial Selection

To select the individuals best suited for the purpose of creating ghosting, it was necessary to compare the resulting image $I_r$ from the convolution of individual with the original artificial image $I_d$

(artificial, plus this defect). This comparison required that the images be on the same size and depth scale. The size scale happened naturaly, bounded by the defined dimensions of the matrices. Ensuring the depth scale was done by windowing the image values. This windowing was performed to ensure that the pixel values of the two images have the same mean and the same standard deviation. To do this:

$$I_c(R,C) = Mean(I_d) + [I_r(R,C) - Mean(I_r)]\frac{StandDev(I_d)}{StandDev(I_r)} \quad (9)$$

Where Ic(R,C) and Ir(R,C) are the pixel values of row R and column C of the corrected and calculated images, respectively.

After ensuring the equality conditions between the images, the comparison between them was made by simple subtraction between one and the other. The average module of each pixel in the matrix resulting from this subtraction was the standard value that quantified the quality of the mathematical process (or the adaptation of the individual), thus the individuals that resulted in the lowest averages were chosen to build the next generation.

### 2.2.3. Crossing over and the next generation

Crossing over, within the present work, consisted of crossing the randomly chosen genes of two individuals, to generate a new and potentially fitter one for convolution, thus creating a "child" of these two individuals. Considering each individual as a K matrix, for each position of this matrix a draw was made with a 50% chance of the value being inherited from the matrix of one of the parents or the other. After the crossing over, small random changes were added to the code of these children. These changes were made by drawing lots for the position in the matrix and a small value to be incremented and/or subtracted. Thus, the new generation composed of individuals theoretically more fit than the previous one was obtained.

## 2.3. Data acquisition and algorithm implementation

The data were acquired in a Bruker M4 Tornado [11] equipment, using a radiographic film as sample and a stainless-steel plate as base. The position of the sample and the base was such that the convergence point between the direction of the detector and X-ray tube was at the base, through the

sample (figure 1B). Radiographic film was used because it was regular, flat, thin, consisted of two far different materials (silver and polyethylene), and because of the amount of data accessible due to previous studies [3]. The steel base was chosen since this material is ease to find and due to the high intensity of the iron peak, an element with characteristic energy within the parameters needed to optimize the image processing tests (Fe-Kα = 6.4 keV). The base was excited by an X-ray beam with a voltage of 50 kV and the mapping was performed with a step of 25 μm and spotsize of 25μm [11]. The resulting map was converted into a gray-scale image with uncompressed TIFF format.

The genetic algorithm processing to find the K matrix was done by considering various ratios μ1/μ2, and visually choosing which value gets the best result when treating the experimentally acquired data. The values used were: 0.16 and 0.83; 0.2 and 0.8; 0.25 and 0.75; 0.33 and 0.66. The simulations were built and run in the Octave language [12]. The displacement of the simulated image for the phantom was 14 pixels (the same as found in the images coming from the equipment), for both row and column. 1300 generations were simulated; in each generation the efficiency and classification tests for each individual considered 100 randomly created images. The efficiency of individuals for each image was calculated as:

$$1 - \text{diff} \tag{10}$$

Where diff is the average of the absolute value of the difference between the original and the simulated image. The total efficiency for each individual is the sum of the efficiencies for each of the 100 randomly created images. The K matrix was simulated with a size equal to 29x29 pixels (2 times the ghost shift plus one unit). The simulation was processed on an Avel i7 computer with 16GB of RAM.

## 3. RESULTS AND DISCUSSION

### 3.1. Obtained matrices and their characteristics.

In figure 5 it is possible to see a certain convergence of the values of the simulations to at least 95% efficiency. This means that the convolution stabilizes by creating images whose pixel values have a maximum variation of 5% from the desired image.

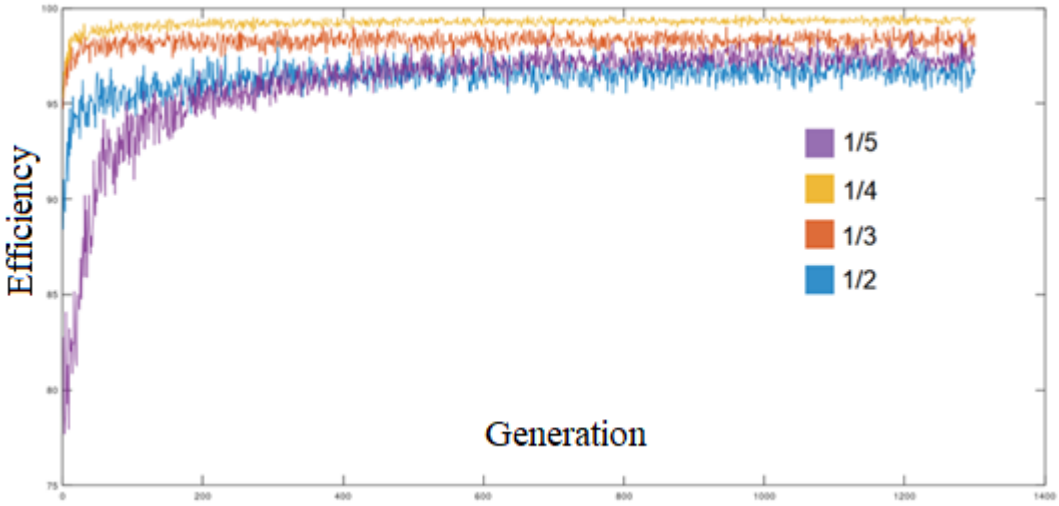


**Figure 5:** Efficiency of the best individual over the 1300 simulated generations. The minimum efficiency in the result is 95% for the case of the 1/2 ratio between μ1/μ2.

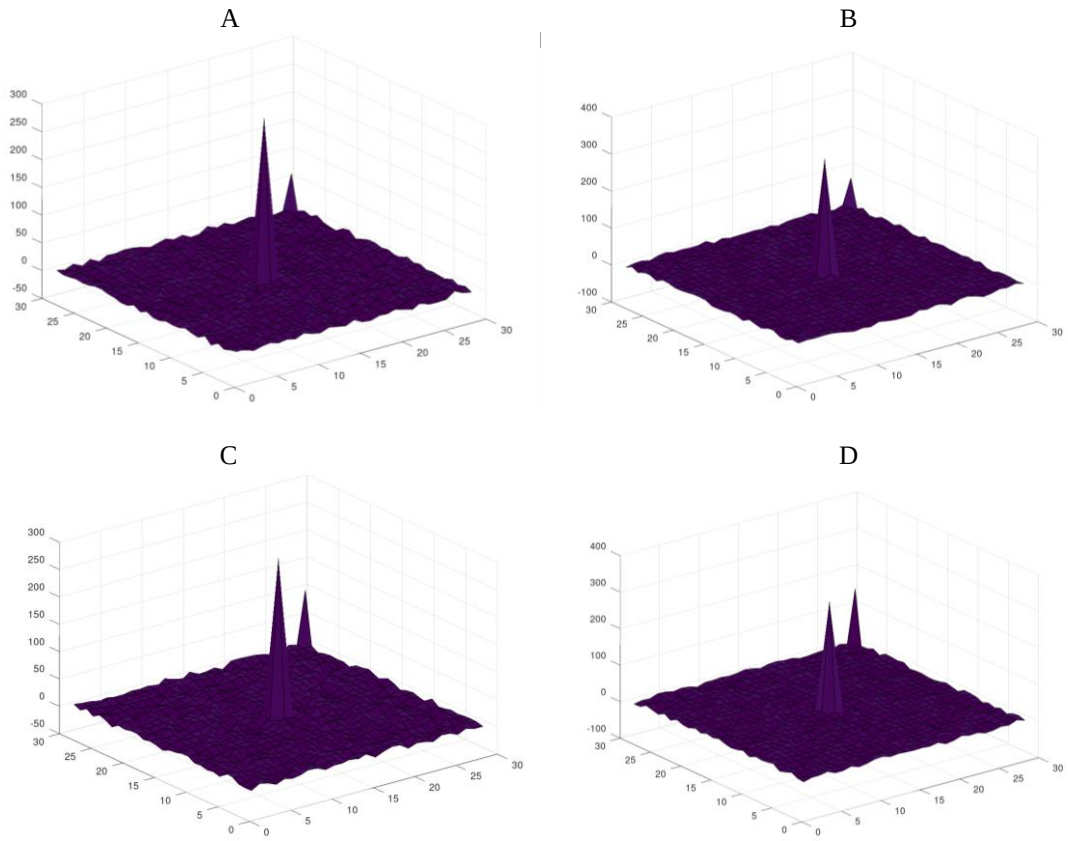


**Figure 6:** Graphical demonstration of the matrix K for (A) 1/5, (B) 1/4, (C) 1/3 and (D) 1/2.

The convolution matrix K appears several values close to zero, and two elements with high values. Since these are large matrices, they are shown graphically in Figure 6, where the dimension z shows the value of the element arranged at position (x, y).

The distance between the peaks is the same as in the image for the ghosting defect, which, in a matrix of zeros, means that the genetic algorithm has chosen the trivial solution to the problem. This is because if equation (8) expanded series considered only in its first order, it becomes:

$$I(R,C) = \mu_1 I_0(R,C) + \mu_2 I_d(R,C) \quad (11)$$

This can be reaffirmed since there is a direct and strong correlation between μ1/μ2 and the intensity of these peaks in the matrix, as shown in Figure 7.

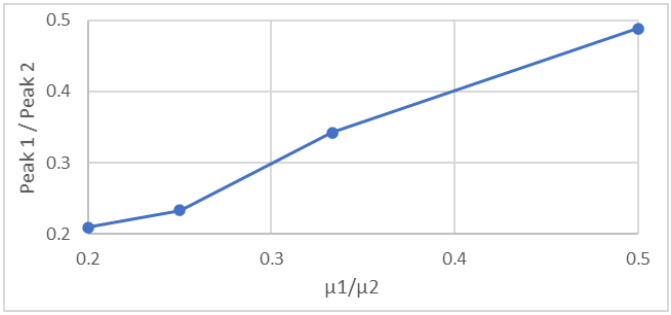


**Figure 7:** Correlation between cell height. The regression returns Y = 0.9616 X + 0.01, where Y is the ratio between the peaks and X the ratio between the attenuation coefficients.

### 3.2. Generalization of the characteristics of matrices and application in real cases.

The matrix K found in each of the situations presents almost all the elements equal to zero, except for two of them. Considering equation 10, it is possible to understand that the central peak creates the "copy" of the original image, and the shifted peak creates the same image, but shifted. In practice, this is a trivial result and allows for a data treatment that is also trivial and easy to generalize: to undo the ghosting defect created by the second peak, it would be enough to convolve by inverting the value of this peak. This would have the opposite effect, removing the ghost image. The only information needed to adjust this procedure is to have knowledge of the ratio between the effective coefficients μ1/μ2, and that this ratio is approximately constant. The result of the image made by mapping the

iron element can be seen in Figure 8. In this case, μ1/μ2 was varied manually, observing the result, and arriving at an optimum situation visually. This situation happened at a ratio of 1/5.

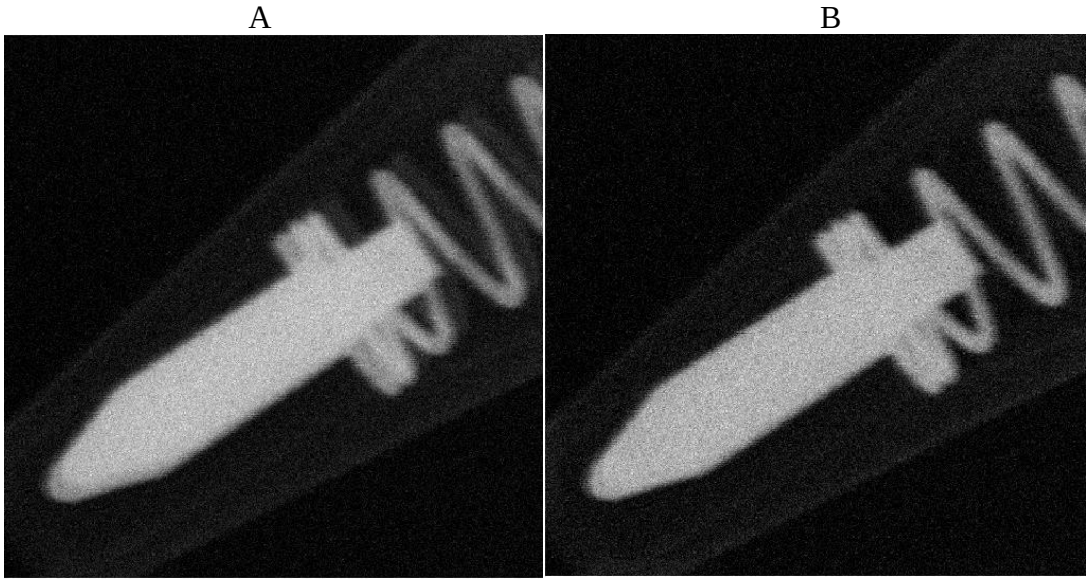


**Figure 8:** Image obtained in the adapted methodology in the equipment, with the characteristic ghosting defect (A) and processed image, after removing this defect (B).

Understanding the logic of the K matrix may be important to circumvent possible side effects of the convolution of the correction matrix. This is because the inverted peak would correct the ghost by adding a "negative" ghost. This procedure can cause a side effect. In this work, the images appear to have enough noise to hide this side effect. If necessary, the correction for this defect can be a third peak, inverted relative to the following to correct the exacerbated subtraction of the negative peak. The matrix for considering this correction, here called second order, can be seen in Figure 9.

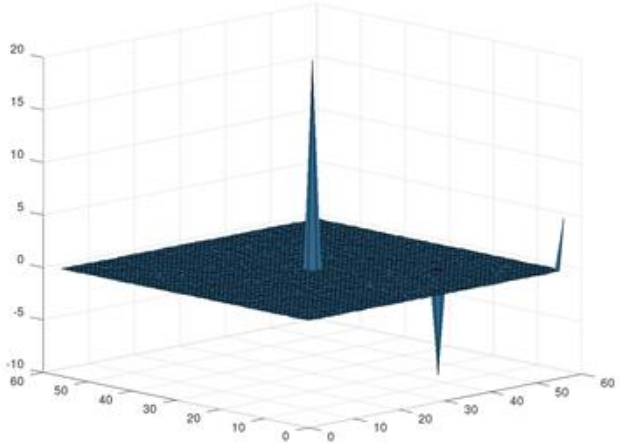


**Figure 9:** Graphical demonstration of the K matrix with second order correction.

It is also possible to do the deconvolution using the found K matrix (figure 10). In this case, Wiener's method [8,9] was used, to perform the inverse operation of equation 1:

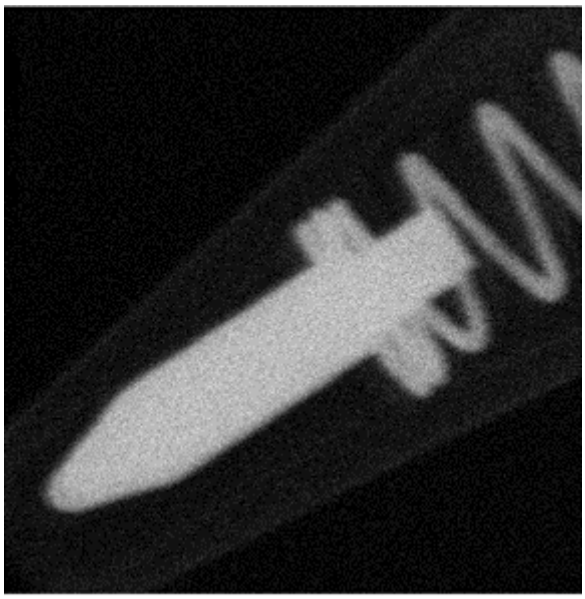

**Figure 10:** Image treated using the K matrix (figure 8A) and the Wiener deconvolution method.

## 4. CONCLUSIONS

The results point out that it is possible to adapt a commercial equipment to do transmittance mapping for thin samples. The choice of to not make mechanical adaptations may have its side effects circumvented by digital processing of the data. It is possible to build an equipment that already has the geometry adapted for this, however, besides being expensive, it will present other problems, such as the difficulty of an angulation for incidence of the beam in a controlled and efficient way. Every way imagined for this adaptation required a greater distance of the detector or tube in relation to the sample, making the efficiency of detection to be impaired.

The restoration of the image in question was successfully achieved. The understanding of the properties of the K matrix makes it possible to apply it, within the problem studied, to all cases in which this type of defect appears in the image. It is possible, from this point on, to study the limits of the application of the results found. The mathematical justification proposed in this work takes into

consideration that the effective values of the attenuation coefficients, or at least the ratio between them, are approximately constant throughout the entire sample.

The genetic algorithm pattern written in this work worked as expected. Although the result of the work was as trivial as possible, it shows a first-order mathematical approximation in equation (8), with satisfactory results when considering the final image. It is possible that further refinement of the simulation could yield better results, with a more complex matrix and considering a second order or even a third order term, but the simulation was successful in its proposal.

The simple pattern found in the K matrix was interesting for the ease of adapting it to the most diverse conditions. It was not necessary to use the path indicated by equation 1 to find the corrected image. The version of GNU Octave used only offers one deconvolution method in two dimensions, the Wiener method [8,9]. The result using this method would be similar to the one found, as shown in Figure 10.

However, it is necessary to consider that the image with the defect has information loss. And that this loss may not be completely restored in the treatment process. This, in practice, could be perceived as a side effect of the linear correction, creating a "negative ghost", i.e. the same defect with inversion of scale. This would be visible mainly where the ratio $\mu 1/\mu 2$ is awfully close to 1. In these cases, a third peak would be necessary, used to soften the exaggerations of the correction caused by the second peak. By logic, the ratio between its values and the second would be the same logic as the ratio between the second and the first. For example, if $\mu 1/\mu 2$ were equal to 0.5, the value of the peaks (with alternating signal), would be 1, 0.5 and 0.25, as would the distance between them. This can be exemplified in Figure 9. In the proportion found in the problem, and due to the noise of the treated image, this correction, for the case treated, proved to be unnecessary.

## ACKNOWLEDGMENTS

This work was developed with internal support from the Federal Institute of Rio de Janeiro (notice 02-2019, PROPPI-IFRJ) with PIBIC scholarships from IFRJ and CNPq. The work also relied on the use of equipment and infrastructure of the State University of Rio de Janeiro and COPPE-UFRJ.

## REFERENCES

[1] AMPTEK. X-Ray Fluorescence (XRF): Understanding characteristic x-rays. **AMETEK Inc**., 2015. 6p. Available: <https://www.amptek.com>. Acessed: July 10th 2021.

[2] SCRUGGD,B.; HASCHKE, M.; HERCZEG, L.; NICOLOSI, J. XRF mapping: new tools for distribution analysis. **Advances in X-ray analysis**, v42, 19-25, 2000.

[3] GONÇALVES, E. A. S.; OLIVEIRA, D. F.; ANJOS, M. J.; ASSIS, J.T.; OLIVEIRA, L.F.; LOPES, R.T. Visualization method for radiographic films through silver intensity mapping using X-ray fluorescence. **X-ray spectrometry**, v. 46, p. 136-141, 2017.

[4] OMAR, D. The analysis of copper-iron metallic mixture by means of XRD and XRF. **International Letters of Chemistry, Physics and Astronomy**, v.64, p.130-134. 2017.

[5] STEPHAN, K.; HIRSCHINGER, M.; MAIER, H.; FRISKE, D. Characterization of thin films by X-ray transmission measurements. **Nuclear Instruments and Methods in Physics Research Section A,** v.397, n.1, p.150-158, 1997.

[6] HUANG, S.; WANG, X.; CHEN, Y.; XU, J.; TANG, T.; MU, B. Modeling and quantitative analysis of X-ray transmission and backscatter imaging aimed at security inspection, **Optics express**, V27, n. 2, p.337-349, 2019.

[7] ALAM, T.; QAMAR, S.; DIXIT, A.; BENAIDA, M. Genetic Algorithm: Reviews, Implementations, and Applications, **International Journal of Engineering Pedagogy**, Preprints, 2020.

[8] GONZALEZ, R.; WOODS, R.; EDDINS, S. **Digital Image Processing Using Matlab**. Prentice Hall, 2003.

[9] OCTAVE FORGE. **Function reference: deconvwnr**. Octave Forge Community, 2020. Available: <https://octave.sourceforge.io/image/function/deconvwnr.html>. Acessed: July 10th 2021.

[10] KNOLL, G. F. **Radiation Detection and Measurement.** New York: John Wiley & Sons, 2010

[11] BRUKER NANO GMBH. **M4 Tornado User Manual**. Berlim: Bruker Nano GmbH, 2013, 165p.

[12] EATON, J. W.; BATEMAN, D.; HAUBERG, S.; WEHBRING, R. GNU **Octave version 5.2.0 manual: a high-level interactive language for numerical computations**. Available: <https://www.gnu.org/software/octave/doc/v5.2.0/> Acessed: July 10th 2021.